SEISMICA

Single-station vehicle tracking using six-component seismic measurements: A comparative study with array-based methods

Shihao Yuan [ID] * [1], **Felix Bernauer** [2], **Joachim Wassermann** [2], **Eileen R. Martin** [1,3], **Heiner Igel** [2]

[1]Department of Geophysics, Colorado School of Mines, Golden, USA, [2]Department of Earth and Environment Sciences, Ludwig-Maximilians-Universität München, Munich, Germany, [3]Department of Applied Math and Statistics, Colorado School of Mines, Golden, USA

Author contributions: *Conceptualization*: SY. *Methodology*: SY. *Software*: SY. *Formal Analysis*: SY. *Investigation*: SY, FB, JW. *Resources*: SY, FB, JW. *Writing - Original draft*: SY. *Writing - Review & Editing*: SY, EM, HI. *Visualization*: SY. *Supervision*: HI, EM. *Funding acquisition*: SY, EM, HI.

Abstract   Determining the direction of seismic waves is crucial for many applications, from monitoring natural hazards like avalanches and landslides to detecting nuclear explosions and conducting surveillance. Traditional methods rely on arrays of seismic sensors arranged in specific patterns, but deploying these arrays can be challenging or impossible in many environments, such as cities, ocean floors, mountains, or other planets. We present an alternative solution: a single-station system that measures six-component (6C) ground motions to determine the direction of seismic sources. Using a collocated seismometer and rotational sensor, we simultaneously record both translational and rotational ground motions to determine the direction of vehicle sources from a single 6C station. The 6C approach not only maintains a small footprint but also extracts directional information from both Rayleigh and Love waves. We validate our method by comparing results from different types of rotational sensors and conventional array-based techniques, including frequency-wavenumber analysis and array-derived rotation. Our findings confirm the 6C method's capability to accurately locate vehicle sources while offering advantages over traditional array deployments, particularly in challenging environments where multiple sensor installations are impractical. The successful application of this method to vehicle tracking demonstrates its versatility beyond traditional seismic studies, opening new opportunities for geohazard early warning systems and urban and environmental seismic noise analysis.

1   Introduction

Seismic-based direction estimation is gaining increasing interest in surveillance systems because of the broadband sensitivities of seismic sensors (Fischer et al., 2013; Wang et al., 2014; Valero et al., 2019; Margheriti et al., 2021). These sensors can detect not only natural events like earthquakes and landslides but also various anthropogenic ground motions, including human and vehicle movements. Recent studies have shown the effectiveness of seismic-based direction estimation across various fields. Avalanche monitoring using seismic sensors has been developed and proven effective at various sites over the past few decades (Almendros et al., 1999; Heck et al., 2019). Riahi and Gerstoft (2015) used an array of geophones to analyze traffic-related signals, demonstrating the usefulness of seismic data for traffic monitoring. Manconi et al. (2016) proposed a real-time method to detect and locate rockslides using seismic records. Additionally, Venkatraman et al. (2011) investigated seismic signals from moving heavy military vehicles to track their movements. Seismic data collected from dense networks has also been used to monitor the evolution of meteorological events, such as rainfall and thunderstorms, with unprecedented detail (Diaz et al., 2023).

The range of applications extends into fields like astrophysics and biology. For instance, Tape et al. (2020) employed seismometers to monitor auroras, while Reinwald et al. (2021) successfully located elephants using seismic sensors, offering new insights into their social interactions. In addition to traditional seismic instruments, more recent technologies like distributed acoustic sensing (DAS) have also been applied for seismic-based direction estimations. Martin et al. (2016) analyzed signals recorded by DAS along highways to locate sources of traffic noise, and Liu et al. (2019) developed a system for vehicle detection and classification using the same DAS technology.

Determining the source directionality of incoming seismic waves is typically achieved through methods such as beamforming or frequency-wavenumber (f-k) analysis (e.g., Krim and Viberg, 1996; Gal and Reading, 2019). These techniques extract coherent seismic energy that propagates to a seismic array based on trial slowness models. Alternatively, polarization analysis can be performed using a single triaxial seismic station, which is effective when pure modes of vibration are present (Greenhalgh et al., 2018).

---

*Corresponding author: syuan@mines.edu

Seismic sensors offer advantages over video or acoustic monitoring systems, as they are less affected by adverse weather conditions or environmental interference (Wang et al., 2014). However, when seismic stations are located very close to surface sources, Rayleigh and Love waves reach these stations almost simultaneously, leading to significant overlap in both the frequency and time domains. This overlap complicates the distinction between these wave types, making it challenging to apply existing techniques for estimating source directionality (Asgari et al., 2015). Additionally, the deployment and maintenance of seismic arrays can be costly. DAS technology provides a more economical alternative, especially when existing fiber-optic cables are used (Lindsey and Martin, 2021). However, its directional sensitivity may limit its ability to detect sources from multiple azimuths. Each of these methods has its strengths and limitations, highlighting the continued need for new methods for seismic source detection and localization.

In this study, we present a six-component (6C) single-station measurement system as an alternative approach for real-time seismic monitoring. This system captures both translational and rotational ground motions, allowing us to track the direction of seismic sources. Our study, conducted at the Geophysical Observatory Fürstenfeldbruck in Germany, begins with a description of the seismic acquisition setup and potential source distributions. We then analyze the recorded signals based on their temporal and spectral characteristics, followed by a demonstration of vehicle tracking using the 6C single-station measurement.

To ensure robustness and accuracy, we validate our results through multiple independent methods. We cross-check the estimated source directionality using two different rotational seismometers (a ring-laser gyroscope and a fiber-optic gyroscope) and compare our findings with array-based techniques, including frequency-wavenumber (f-k) analysis and array-derived rotation (ADR). While Yuan et al. (2020a) introduced the 6C method for earthquake rupture tracking using primarily synthetic examples and limited real data from a single wave type and station, this study advances that work through three key aspects: (1) testing of emerging portable rotational sensors, (2) making use of multiple 6C observations, and (3) cross-validating results with nearby permanent and temporary broadband seismometers. Our validation strategy, employing various methods, wavefields, and sensor types, thoroughly evaluates the advantages and limitations of the 6C measurement technique. The results demonstrate its potential for tracking various seismic and natural sources, particularly in scenarios where traditional array deployment is impractical.

2   Data acquisition

In combination with a classic three-component (3C) broadband seismometer, the newly built ring laser gyroscope (named ROMY) at the Geophysical Observatory Fürstenfeldbruck N 48.164234°, E 11.275865°) near Munich, Germany, allows us to record additional, accurate,

and broadband 3C rotational ground motions (Fig.1). This setup enables simultaneous 6C recordings, i.e., 3C translational and 3C rotational motions, satisfying the requirements for geodetic and seismic observations at various scales (Gebauer et al., 2020; Igel et al., 2021). ROMY is a tetrahedral-shaped four-component rotational sensor (one auxiliary vertical component aligned on the horizontal surface) with each triangular side being approximately 12 m. FUR is a permanent station, belonging to the German Regional Seismic Network, equipped with a Streckeisen STS-2 sensor and a REFTEK RT130 datalogger. FUR and ROMY are just a few meters away from each other and thus are treated as a single 6C station. TON and FFB2–3, also serving as permanent stations, are particularly chosen to identify train- and car-related seismic signals considering their relative locations to the railway and highway nearby (blue and green curves shown in Fig. 1). For verification of the proposed 6C single-station measurements, we deployed a small seismic array comprising seven broadband sensors (Trillium Compact 120s), designated as DROMY and DRMY1–6, which enabled f-k analysis. Additionally, we established two temporary 6C stations (BS1 and BS2), each equipped with a collocated broadband seismometer (Trillium Compact 120s) and a portable fiber optic gyroscope (Exail, formerly iXblue, blueSeis-3A). The ROMY ring laser gyroscope was used in conjunction with the blueSeis-3A rotational sensors at stations BS1 and BS2 to cross-validate the vehicle monitoring capabilities of the 6C method.

3   Traffic signal classification

The amplitude and frequencies of traffic-related seismic signals are primarily influenced by engine vibrations, vehicle speeds, and road conditions, generating both Rayleigh and Love waves in the range of approximately 2 to 50 Hz (Nakata, 2016; Díaz et al., 2017; Fuchs and Bokelmann, 2018). Raw particle velocity recordings sampled at 100 Hz from seismometers are corrected for instrument response, detrended, and converted to particle acceleration. The vertical component of continuous acceleration data (Az) from 01:00 a.m. to 02:00 a.m. is presented in Fig. 2 for stations TON, FFB2–3, DROMY, and DRMY1–6. We select this midnight period to minimize potential overlaps caused by heavy traffic or other human activities during the day. Notably, similar events are recorded at all stations except TON, which can be attributed to their relative locations and distinct dominant signal sources.

As shown in the site map of Fig. 1, all seismic stations, including ROMY, are near the highway, except for station TON, which is closer to the railway. Besides the prominent event around 400 s at station TON, caused by a freight train, we also observe weaker events around 1400 s and 1750 s, likely attributed to commuter trains (Fig. 2). To further analyze the signals, we extract two segments of data within the red dashed squares in Fig. 2 and present their time-frequency characteristics in Fig. 3.

The top panel displays train-related signals recorded at the station pair TON–FFB3, along with their corre-
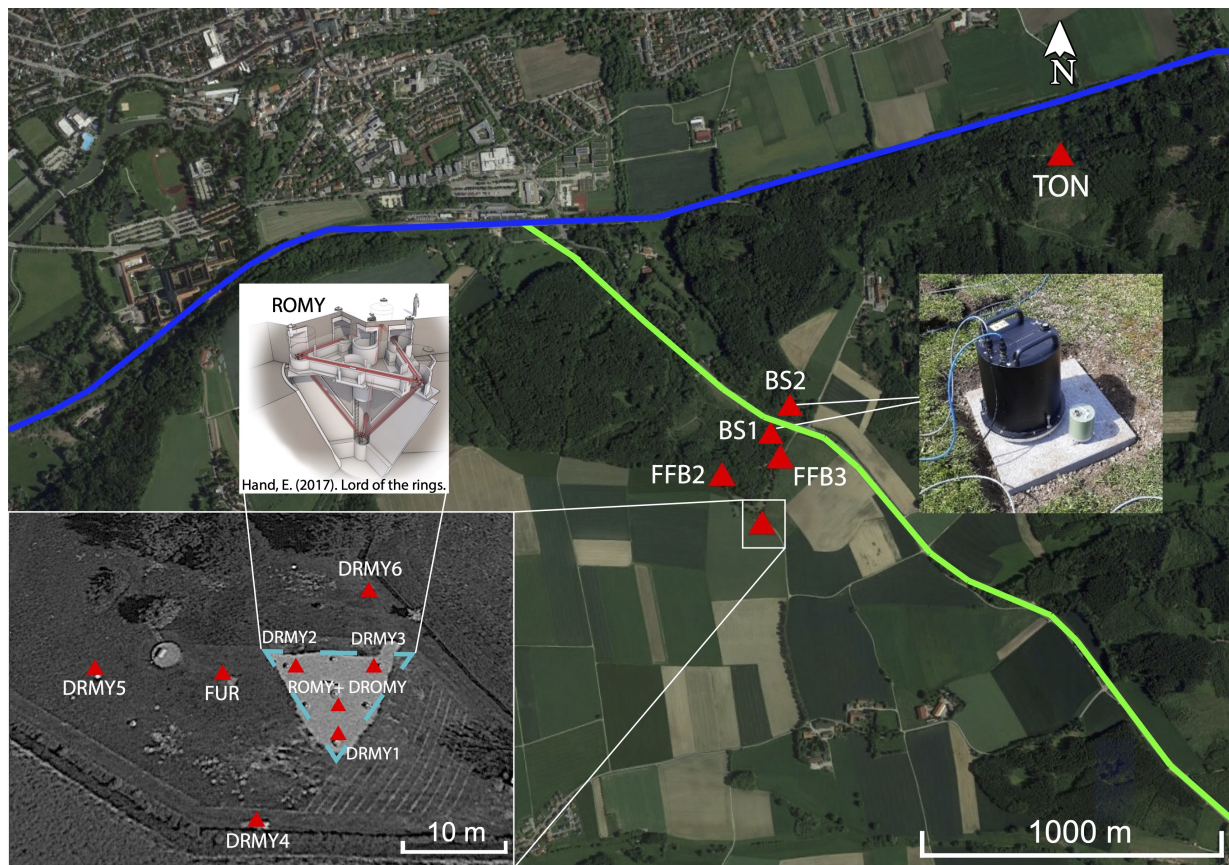
Figure 1 The site map and acquisition geometry at the Geophysical Observatory Fürstenfeldbruck (N 48.164234°, E 11.275865°), Germany, are shown here. Red triangles represent seismic stations. The bottom-left zoomed-in plots highlight the position of the 6C station (FUR+ROMY, with ROMY indicated by the blue dashed triangle) and the inner array (DROMY and DRMY1–6) used for frequency-wavenumber (f-k) analysis alongside stations FFB2–3. The upper-right zoomed-in plot shows the two additional 6C stations, BS1 and BS2, each equipped with portable sensors: a collocated seismometer (in grey) and a blueSeis-3A rotational sensor (in black). Aside from ROMY and blueSeis-3A, which are a ring laser and a fiber optic gyroscope recording rotational ground motions, all other stations are triaxial broadband seismometers capturing translational ground motions. Blue and green curves denote the train track and highway near the observatory, respectively.

sponding spectrograms (Figs. 3a–b). The arrival time difference of the peak ground motions at two stations is approximately 30 s and can be attributed to the traveling time of the freight train from the nearest point of one station to the other. The waveform amplitude at station FFB3 appears less pronounced than at TON, likely due to rapid attenuation of high-frequency components. However, lower resonance frequencies at FFB3—specifically 5, 9, 12, and 14 Hz—are retained and correspond to those detected at station TON. Furthermore, at TON, specific monochromatic spectral lines are observed at approximately 16, 26, 37, and 45 Hz. These resonant frequencies are likely caused by mechanical vibrations from a pump located near the measurement site.

The bottom panel of Fig. 3 presents car-related signals recorded at stations FFB2 and FFB3. The amplitude and arrival time difference of these signals are less pronounced than those at stations TON and FFB3, likely due to their closer proximity. Common features in the spectrograms shown in Figs. 3c–d indicate that both signals originate from the same sources. The lack of higher frequency components (above 20 Hz) at station FFB2, compared to FFB3, is primarily attributed to attenuation, similar to what is observed with the train signals

at station FFB3.

4 Tracking vehicle sources using 6C single-station measurement

The capability of 6C single-station measurements in estimating earthquake back-azimuth (Baz) has been demonstrated in several studies (e.g., Igel et al., 2007; Hadziioannou et al., 2012; Yuan et al., 2020a; Chen et al., 2023). The key principle underlying this method is that the rotational sensor acts as a polarization-propagation filter. This filter not only eliminates longitudinal waves but also separates SV- and SH-type ground motions into horizontal and vertical rotational components, respectively.

4.1 6C single-station measurement using Love waves

When focusing on SH and/or Love waves in an isotropic medium, we can exclusively analyze the vertical component of rotational motions. The Baz estimation process involves rotating the horizontal translational components through a range of trial Baz values (0° to 360°) to obtain radial and transverse components. We then
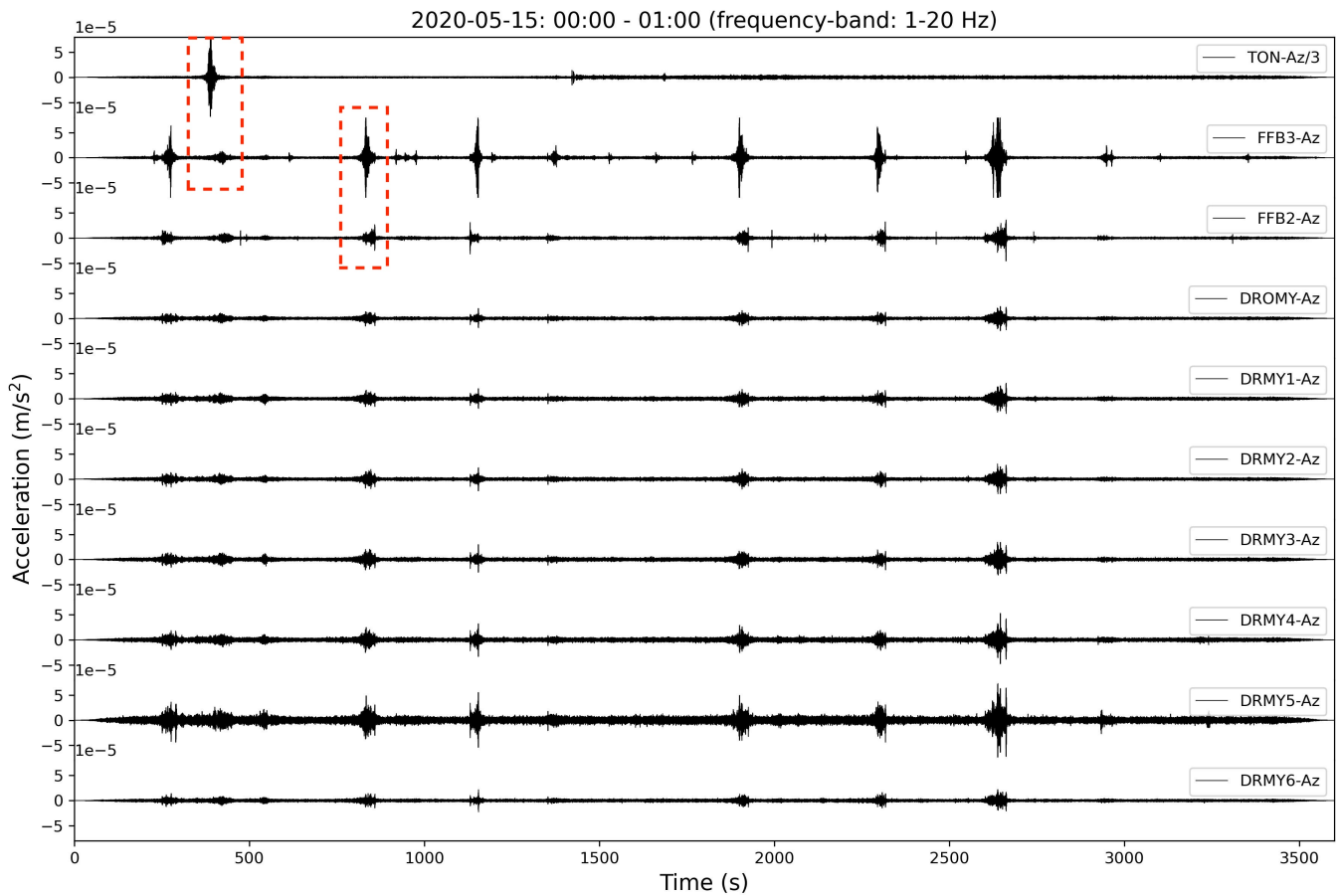
Figure 2 Traffic-induced seismic signals recorded by the seismometers shown in Fig. 1 from 1:00 a.m. to 2:00 a.m on May 15, 2020. The vertical component of the raw particle velocity records from the seismometers has been corrected for instrument response, detrended, converted to particle acceleration, and band-pass filtered into 1-20 Hz. All waveforms are plotted to the same scale, except for station TON, where the waveform amplitude has been divided by a factor of 3. The spectrograms for the waveform enclosed by the red dashed square are shown in Fig. 3.

calculate the zero-lag cross-correlation (CC) coefficient between the transverse acceleration (At) and vertical rotational rate (Rz) for each trial Baz. Assuming that the cross-correlation between Love and Rayleigh waves is significantly smaller than the variance of Rayleigh waves, the CC coefficient reaches its maximum when the trial Baz aligns with the actual Baz, as both represent the same portion of ground motion. Importantly, this 6C approach resolves the 180° ambiguity inherent in conventional 3C single-station methods without the need for prior knowledge of the source focal mechanism, by analyzing the relationship between rotational and translational motions. We apply the CC-based algorithm to the same period of data shown in Fig. 2 for the ROMY 6C station, with the results presented in Figs. 4a–d. We also analyze a different time period for the BS1 6C station, with results shown in Fig. 5.

Given the relative position of the 6C stations and the highway (Fig. 1), we expect the Baz variations of inbound vehicles (moving from southeast to northwest) to decrease from 100° to 0° and then continue decreasing from 360° to 300°. The patterns for outbound vehicles will be the reverse. Although the ROMY and BS1 6C stations collect data from different time periods, the retrieved Baz should exhibit similar patterns of variations due to their relative locations to the high-

way (Fig. 1). Fig. 4d and Fig. 5c demonstrate the comparable bi-directional variation patterns in the estimated Baz for the ROMY 6C station and the BS1 station, respectively. For the cross-correlation (CC) analysis, we use a 10-second sliding window for the ROMY station and a 1-second sliding window for the BS1 and BS2 stations. The shorter 1-second window at BS1 and BS2 is chosen because these stations are closer to the source, leading to faster-varying source signals. This allows for better temporal resolution in capturing the more rapidly changing motion at these locations. In contrast, the longer 10-second window at ROMY is used to ensure more stable measurements, as it is further from the source, where the motion is expected to vary more slowly. The difference in window lengths balances the need for higher resolution in the faster-varying source signals at BS1 and BS2 with the potential for increased noise and overlapping signals in shorter windows. We apply 95% overlap for the sliding windows and retain only Baz values with a CC coefficient higher than 0.4 to reduce interference from signals with low signal-to-noise ratios.

From the zoom-in plots of two selected time windows within the red squares in Fig. 4d at station ROMY, we can calculate the moving speeds of vehicles through the ratio of distance and time over a certain Baz variation
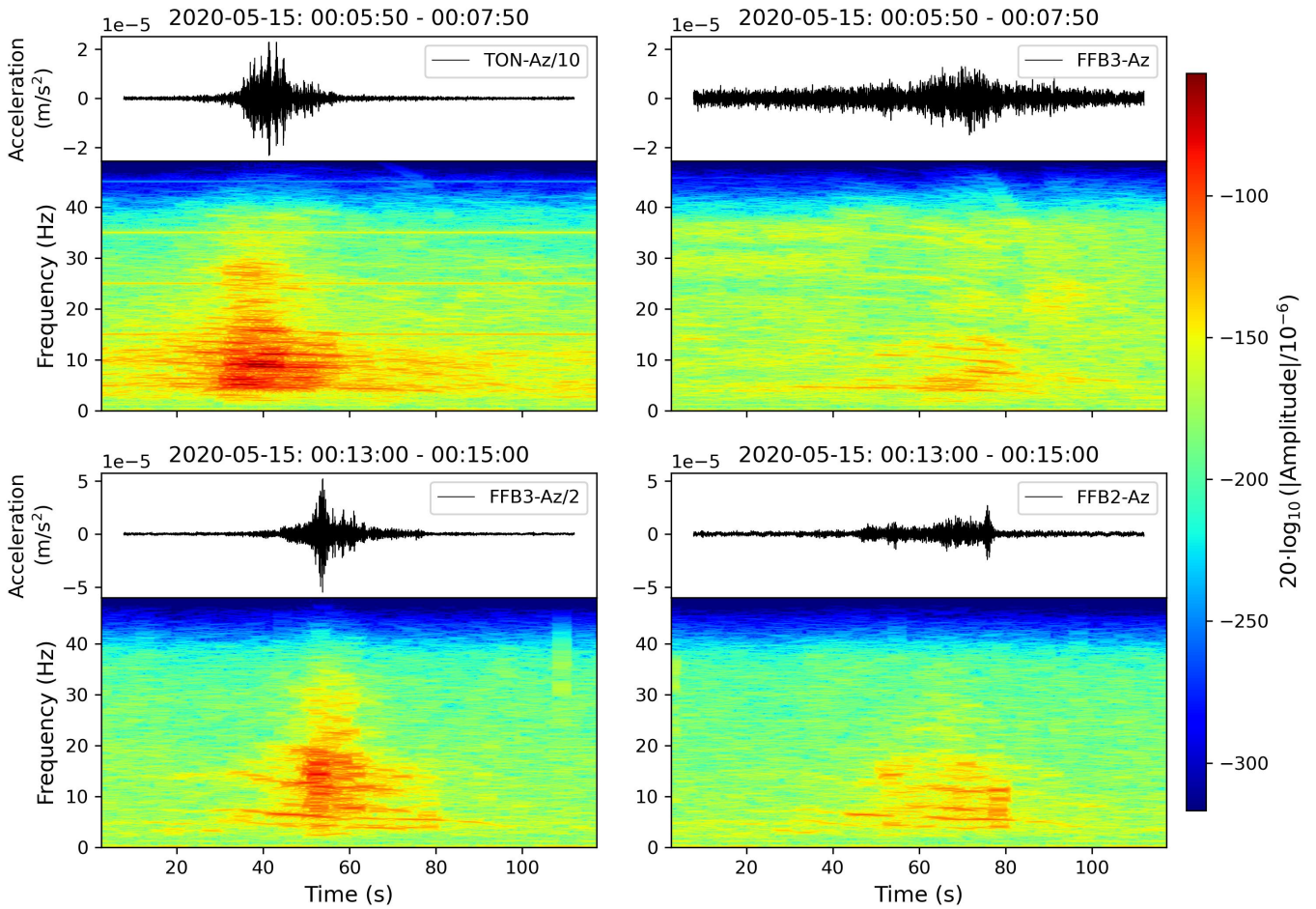
Figure 3 Vertical components of acceleration waveform and spectrograms of the train- (a–b) and car-induced (c–d) seismic signals recorded by the TON, FFB3, and FUR stations. The waveform amplitude at station TON is divided by a scaling factor of 10 in (a) and FFB3 is divided by 2 in (c) for visualization purposes.

range. The estimated average speed in Fig. 4f for the Baz changing from $80°$ to $0°$ is approximately 90 km/h and the one in Fig. 4g is approximately 65 km/h. Both estimates are considered empirically reasonable for this time of night. The smaller slope of the Baz variation between $0°$ and $30°$ is thought to be associated with potential braking operations related to a road exit.

4.2 6C single-station measurement using Rayleigh waves

Our approach goes beyond just using SH-type waves. We also use SV and Rayleigh waves generated by moving vehicles, which can be detected through their horizontal rotational components. This approach is akin to the polarization analysis of P waves with a conventional triaxial seismometer, as P and SH-type waves are not included in the horizontal rotational components. Specifically, we start by conducting a polarization analysis using singular value decomposition (e.g., Gal and Reading, 2019) and then calculate the polarization angle between the two rotational components using the following equation:

$$\theta_{Baz} = -\arctan\left(\frac{\dot{R}_n}{\dot{R}_e}\right), \qquad (1)$$

where $\dot{R}_n$ and $\dot{R}_e$ denote the north-south and east-

west components of rotational rate, respectively. The θ_{Baz} value derived from the inverse tangent function is between $0°$ and $180°$. To remove the $180°$ ambiguity, we then compare the rotated transverse component of rotational rate ($\dot{R}_t$) based on θ_{Baz} with the vertical component of acceleration (A_z) through zero-lag CC. If the CC coefficient is positive, $180°$ should be added to θ_{Baz}.

As the horizontal rotational components of ROMY were under technical maintenance during the period that we deployed the temporal array (DROMY and DRMY1–6), we chose another chunk of data a year ago (from 00:00 a.m.–01:00 a.m., May 15, 2019) as shown in Figs. 6a–c. In spite of the date difference, we expect to see similar bi-directional patterns for the Baz estimate due to the generally unchanged road condition. The horizontal rotational motions (Re and Rn) are noisier than acceleration and vertical rotational motions (Rz). The glitches and spurious events in Fig. 6c mostly result from mode jumps of the laser due to the unstable cavity length and/or outgassing effect.

The estimated Baz at the ROMY 6C station from Re/Rn and Az components using the polarization method and Rayleigh waves described above is shown in Fig. 6e, while that from Ae/An and Rz components using CC method and Love waves is shown in Fig. 6d for comparison. Despite the relatively low signal-to-noise ratios
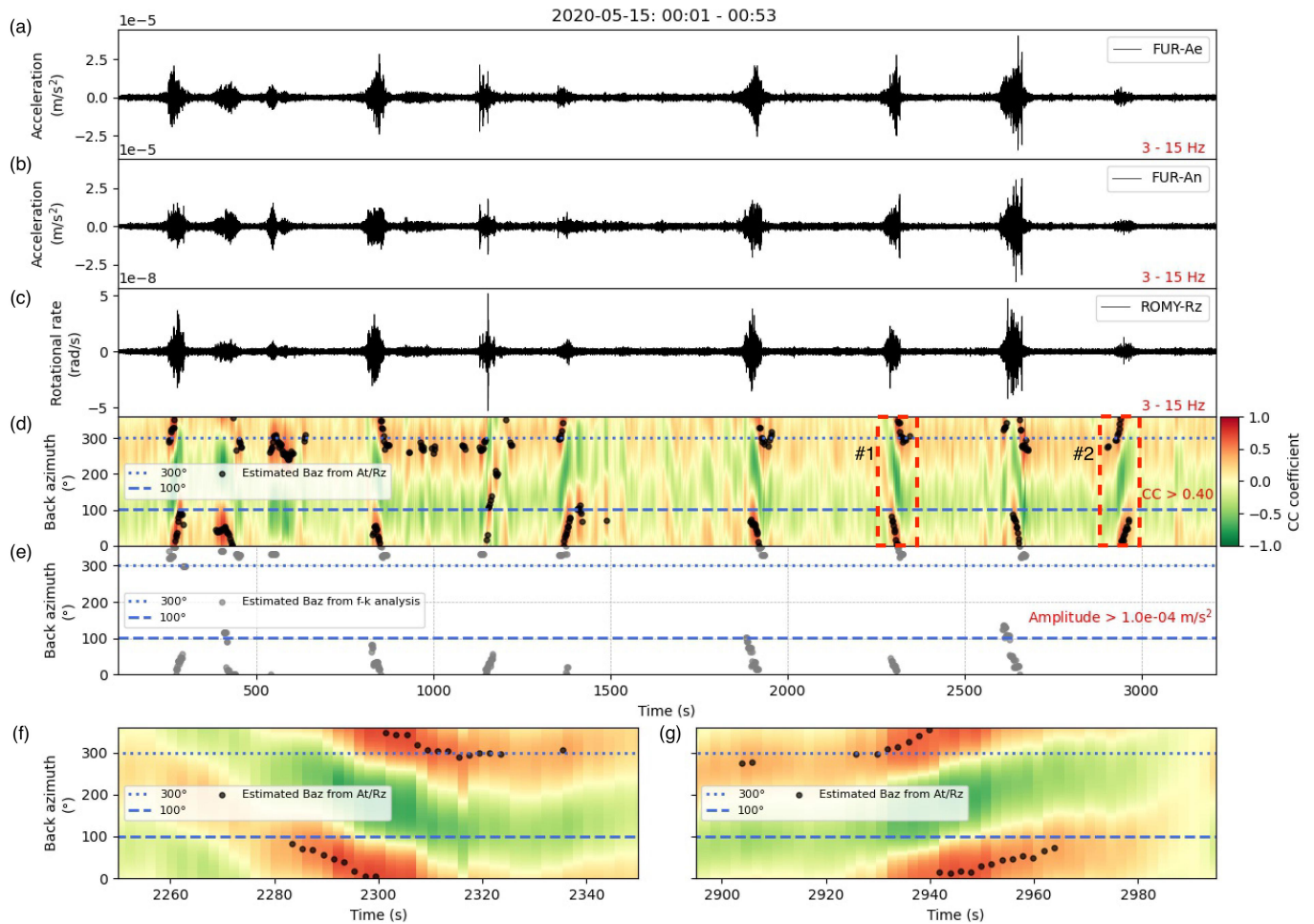
Figure 4 Back azimuth (Baz) estimation of the car-induced Love waves from 6C single-station measurement at station ROMY. The north-south (a) and east-west (b) components of acceleration at FUR station. (c) The vertical rotational rate at ROMY station. (d) Estimated Baz from Ae/An and Rz components using CC method. (e) Estimated Baz from the f-k analysis. The background colors represent CC coefficients and the dots in (c) and (d) denote the estimated Baz for each sliding window with a CC coefficient higher than 0.3 and maximum amplitude larger than $10^{-4}\ m/s^2$, respectively. (f) and (g) correspond to the zoom-in plots within #1 and #2 red squares in (d), respectively.
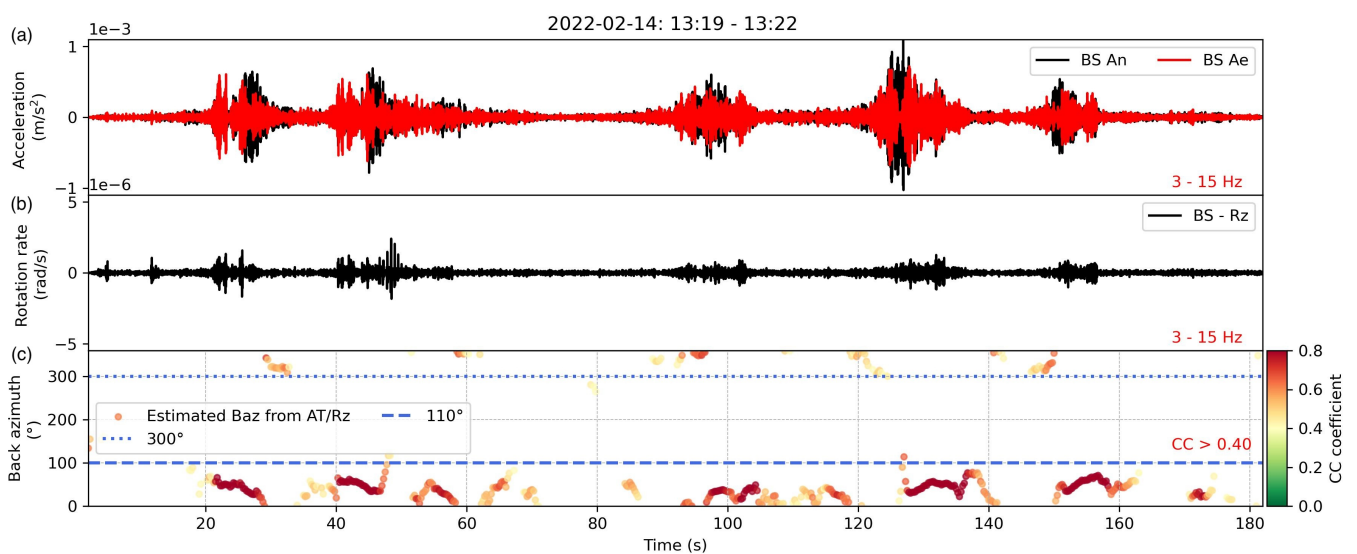

Figure 5 Back azimuth (Baz) estimation of the car-induced Love waves from 6C single-station measurement at station BS1. (a) The north-south (An) and east-west (Ae) components of acceleration. (b) The vertical component of rotational rate (Rz). (c) Estimated Baz from Ae/An and Rz components using CC method and Love waves. The color of the dots represents the CC coefficients higher than 0.4.

of Re and Rn components, we could still identify consistent Baz variation patterns within certain time windows. When the stability of horizontal rotational components of ROMY gets improved in the future, we expect better agreement.

In contrast to the ROMY station, the horizontal component of the portable rotation sensor at the BS1 and BS2 stations does not experience instrumental instability. We can clearly observe Baz variations due to moving vehicles (Fig. 7c). The retrieved Baz primarily relies on Rayleigh waves since we are using horizontal rotational components. The results are consistent not only with the Baz derived from Love waves at the same station (Fig. 5) but also with those obtained from the ROMY station (Fig. 6). By comparing the peak amplitudes of the horizontal and vertical components of rotation at the BS1 station (Figs. 5a–b and Figs. 7a–b), we can find that the car-induced Rayleigh waves exhibit higher signal-to-noise ratios. This allows for more stable and robust Baz estimation through polarization analysis of the horizontal components of the rotational recordings.

5 Tracking vehicle sources using frequency-wavenumber analysis

A practical way to validate the proposed 6C single-station measurement is to use a seismic array, which can deliver similar information. Array-based beam-forming or frequency-wavenumber (f-k) analysis, a technique that decomposes seismic signals into their spatial and temporal components, is commonly employed for wave-type identification, source direction estimation (i.e., Baz), and slowness estimation of incoming waves. By examining the coherence and phase relationships between array sensors, f-k analysis is used to characterize the propagation characteristics of seismic waves, enabling the estimation of wave velocity and direction of arrival. A detailed description of the methodology can be found in Gal and Reading (e.g., 2019). Ideally, we should achieve very similar temporal variations of the seismic source Baz through both array and single-station measurements. Therefore, we deployed a small-scale seismic array (DROMY and DRMY1–6 shown in the zoom-in plot of Fig. 1) around the 6C station. Alongside the permanent stations FFB1 and FFB2, we applied f-k analysis to the array data over the same time period of Fig. 4 to estimate Baz using a consistent sliding window. One challenge in applying f-k analysis to Love waves is the potential mixing of Rayleigh and Love waves when tracking moving seismic sources using horizontal components. Therefore, we restrict the f-k analysis to the vertical component of the array recordings for Rayleigh waves.

In Fig. 4e, we exclude samples of the estimated Baz with a maximum amplitude smaller than $1.0e^{-4}$ m/s^2 within the corresponding time window. There is a strong agreement between the Baz variations obtained from the 6C measurement (Fig. 4d) and the f-k analysis (Fig. 4e). The difference between Fig. 4d and 4e can be mainly attributed to three factors. First, the array-based f-k analysis relies on SV/Rayleigh waves, as it uses

the vertical components of acceleration, while the 6C single-station analysis is based on SH/Love waves. The radiation patterns of these different wave types may vary, resulting in unequal signal-to-noise ratios within the same time window. Second, we filter the estimated Baz using the cross-correlation coefficient for the 6C analysis, whereas in the f-k analysis, we apply an amplitude threshold. Third, the geometry of the array affects the resolution capabilities of the f-k analysis, which may also contribute to discrepancies between the two measurement methods. These factors combined may explain the differences observed when comparing the f-k and 6C single-station measurements.

6 Tracking vehicle sources using array-derived rotation

Rotational motions can essentially be represented by spatial gradients of translational motions, allowing us to calculate them indirectly using closely spaced triaxial seismometers (e.g., Spudich et al., 1995). This approach is known as array-derived rotation (ADR). Despite its band-limited accuracy (Langston, 2007), ADR provides an independent way to validate rotational motions recorded directly by rotational sensors. To verify the proposed 6C single-station measurement, we first compute the three components of ADR for the reference station DROMY using data from the surrounding stations DRMY1–3 (Figs. 8b–c). We then apply the same processing strategy outlined in Section 4 to both the ADR and acceleration records at station DROMY. As shown in Figs. 8d–e, the estimated Baz variations from SH/Love waves (At/Rz) and SV/Rayleigh waves (Re/Rn) are not only consistent with each other, but also align well with those obtained from the 6C single-station measurement at stations ROMY and BS1 (Figures 4-7).

7 Tracking vehicle sources using multiple 6C stations

A single 6C station can track moving vehicles if their path is known, as the real-time source location is determined by the point where the calculated back azimuth intersects that path. When multiple 6C stations are used, we can locate sources without prior knowledge of their path. While Yuan et al. (2020a) demonstrated this concept using synthetic data for earthquake rupture tracking, our study extends this work by applying and validating the 6C method using real data from multiple stations to track moving vehicles.

We use two 6C stations (BS1 and BS2) on opposite sides of the highway, as illustrated in Fig. 1. Our analysis focuses on Rayleigh waves recorded by the horizontal components of the rotational sensors, following the method detailed in Section 4.2. These horizontal components were chosen for their superior signal-to-noise ratios compared to the vertical component. For source tracking, we project each station's estimated back azimuth as a directional beam, calculating beam amplitudes using the shape function from Equation 3 of Yuan et al. (2020a). To demonstrate the effectiveness of vehi-
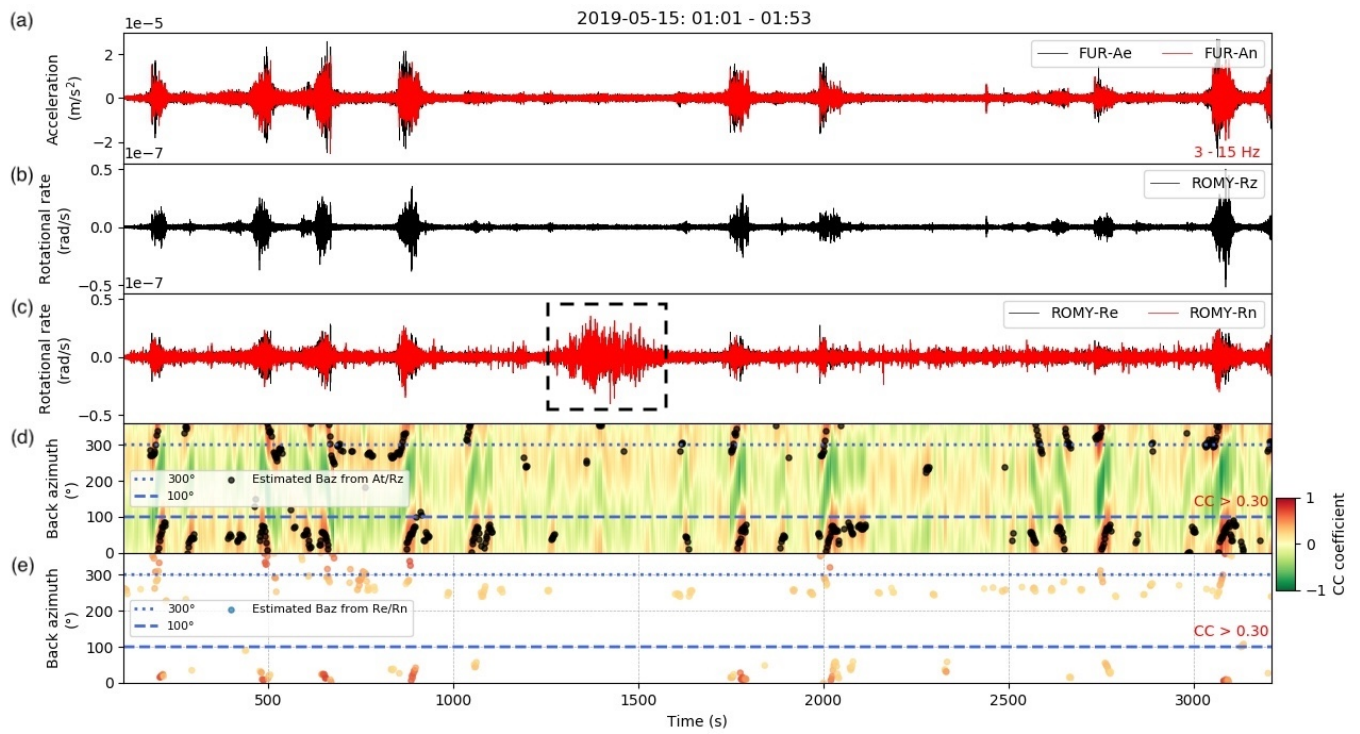
Figure 6 Back azimuth (Baz) estimation of the car-induced Rayleigh and Love waves from 6C single-station measurement at station ROMY. (a) The north-south (red) and east-west (black) components of acceleration at station FUR. (b) The vertical rotational rate at station ROMY. (c) The north-south (red) and east-west (black) components of rotational rate at station ROMY. The black dashed square represents a spurious event caused by instrumental instability. (d) Estimated Baz from Ae/An and Rz components using CC method focusing on Love waves. (e) Estimated Baz from Re/Rn and Az components using polarization method focusing on Rayleigh waves. The background colors represent the correlation coefficient (CC) values, while the dots indicate the estimated Baz for each sliding window with a CC coefficient above 0.3. The correlation coefficient threshold of 0.3 was chosen to enhance the visualization of variations in the estimated source directions. This threshold helps to filter out noise, ensuring that only relevant signals are considered.
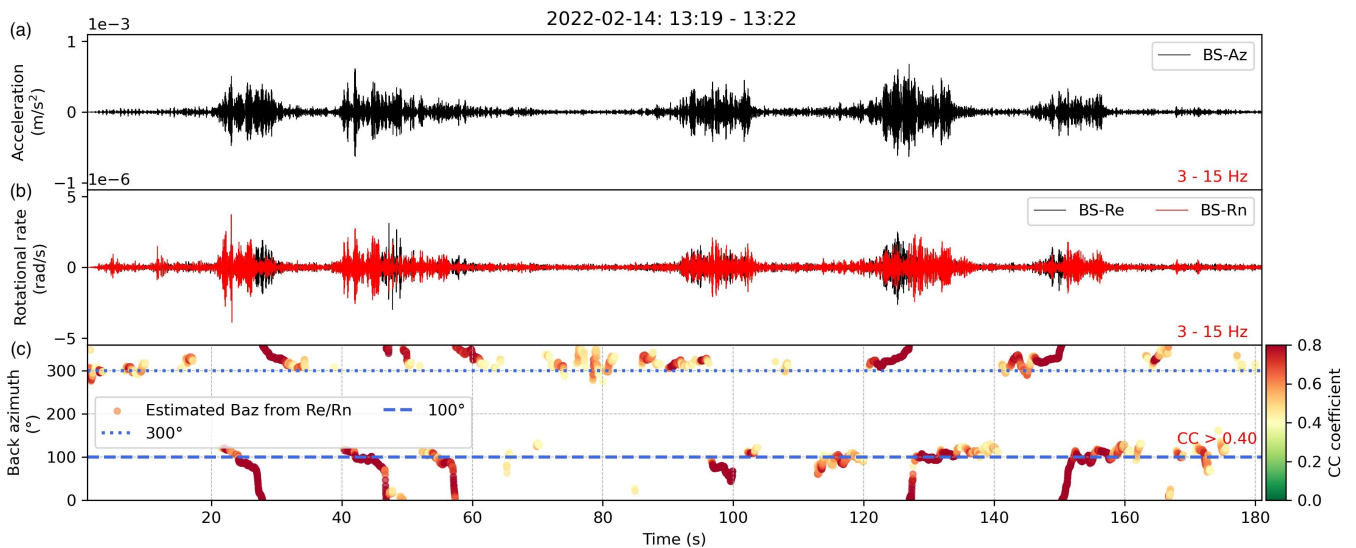

Figure 7 Back azimuth (Baz) estimation of the car-induced Rayleigh waves from 6C single-station measurement at station BS1. (a) The vertical component of acceleration (Az). (b) The north-south (Rn) and east-west (Re) components of rotational rate. (c) Estimated Baz from Re/Rn and Az components using polarization method and Rayleigh waves. The color of the dots represents the CC coefficients higher than 0.4.

cle tracking using multiple 6C stations, we present three representative time windows. Fig. 9 presents the results: the top and middle panels show horizontal rotational recordings from BS1 and BS2, respectively, while the bottom panels display the projected source directions from each station. Comparing these projections with the highway's path (marked by white curves) reveals that the vehicle was traveling southbound. We ob-
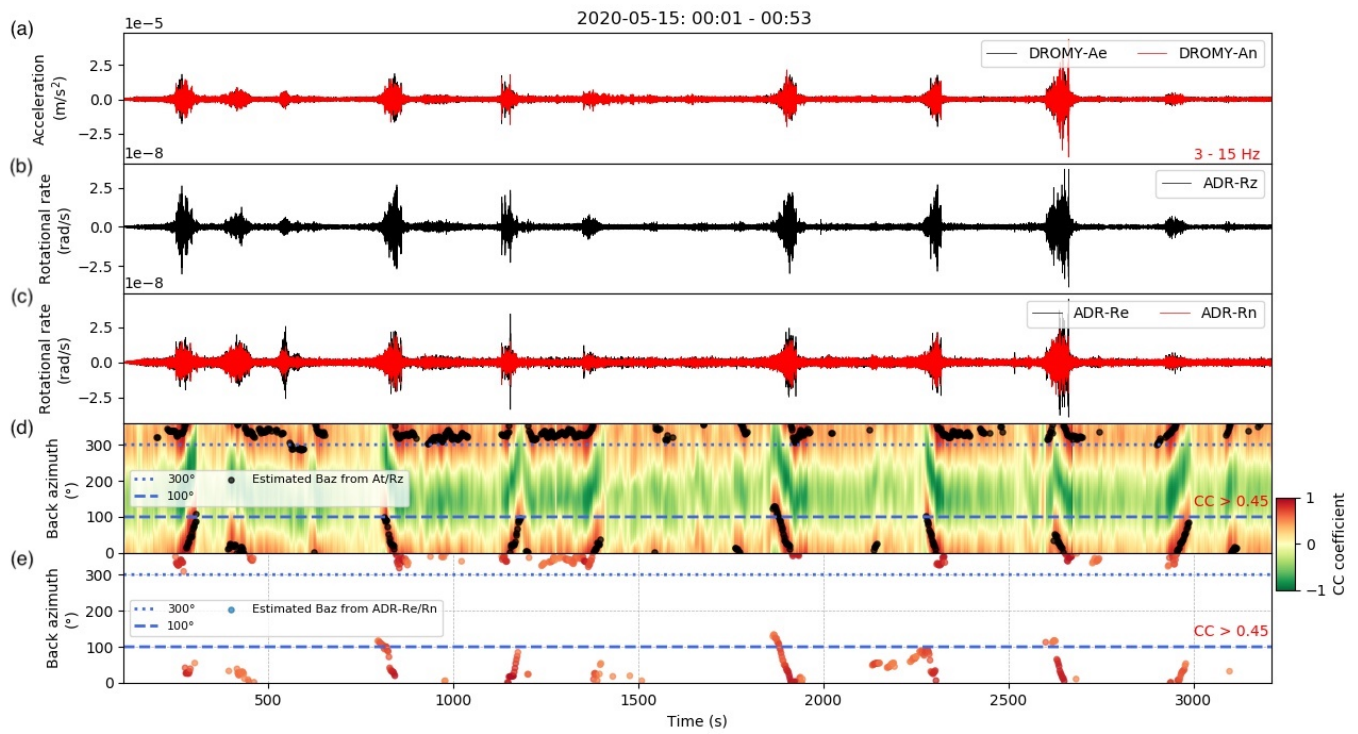
Figure 8 6C measurement applied onto array-derived rotation (ADR). (a) The north-south (An) and east-west (Ae) components of acceleration at DROMY station. (b) The vertical component of array-derived rotational rate (Rz) at DROMY station. (c) The north-south (Rn) and east-west (Re) components of array-derived rotational rate at DROMY station. (d) Estimated Baz from Ae/An and array-derived Rz using CC method focusing on Love waves. (e) Estimated Baz from array-derived Re/Rn and Az components using polarization method focusing on Rayleigh waves. The background colors represent CC coefficients and the dots denote the estimated Baz for each sliding window with a CC coefficient higher than 0.45.

serve a slight misalignment between the located moving cars and the driveway in the bottom panels of Figure 9. This misalignment may be primarily due to two factors. First, the synchronized time windows from the two 6C stations may not capture car signals originating from the exact same location, given the unequal source-receiver distances. Second, there may be an installation misalignment at stations BS1 and BS2 between the seismometer and the rotational seismometer, introducing errors in the estimation of incoming wave directions.

8 Discussion

Although this study concentrates on traffic signals, the 6C measurements have the potential for wide applicability to various seismic sources in both urban and natural environments. The seismic source we refer to here is any source that can generate ground vibrations that seismometers can detect. Analyzing these diverse source distributions could enhance our understanding of natural processes such as river sediment transportation and bedrock erosion (Burtin et al., 2010), Earth-ocean-atmosphere interactions (Kedar and Webb, 2005). It could also provide insights into geological phenomena including volcanic activities (Brenguier et al., 2011; Obermann et al., 2013) and earthquakes (Hadziioannou et al., 2011; Obermann et al., 2014). Furthermore, this technique shows promise for monitoring natural hazards like landslides (Suriñach Cornet et al., 2005; Tonnellier et al., 2013) and hurricanes (Davy et al., 2014; Fan

et al., 2019). The rotational components of 6C measurements naturally separate Rayleigh and Love waves, potentially enhancing detection, classification, and monitoring of diverse seismic events based on their time and frequency characteristics.

Ground vibrations from various sources provide valuable data for inferring near-surface structures. By determining the directionalities of both static and dynamic sources, we effectively transform passive seismic experiments into active ones. Moving objects, such as vehicles, can be considered as moving impulse sources that continuously generate ground shaking with varying azimuth and distance. Recent studies have shown that 6C measurements can extract surface wave dispersion characteristics and invert for shear-wave profiles (e.g., Wassermann et al., 2016; Keil et al., 2021). The continuous nature of many anthropogenic and natural sources allows for potential monitoring of dynamic changes in subsurface structures over time, complementing conventional active and passive techniques, especially in complex geological and urban settings.

Traditional three-component single seismic station can be used to estimate attenuation parameters from traffic noise, which is crucial for near-surface characterization (Zhao et al., 2023). With a 3C single seismometer, the attenuation model is often simplified as frequency-independent, a useful approximation particularly at low frequencies. However, using the proposed 6C method, which naturally separates wave types and retrieves dispersion information from both Rayleigh
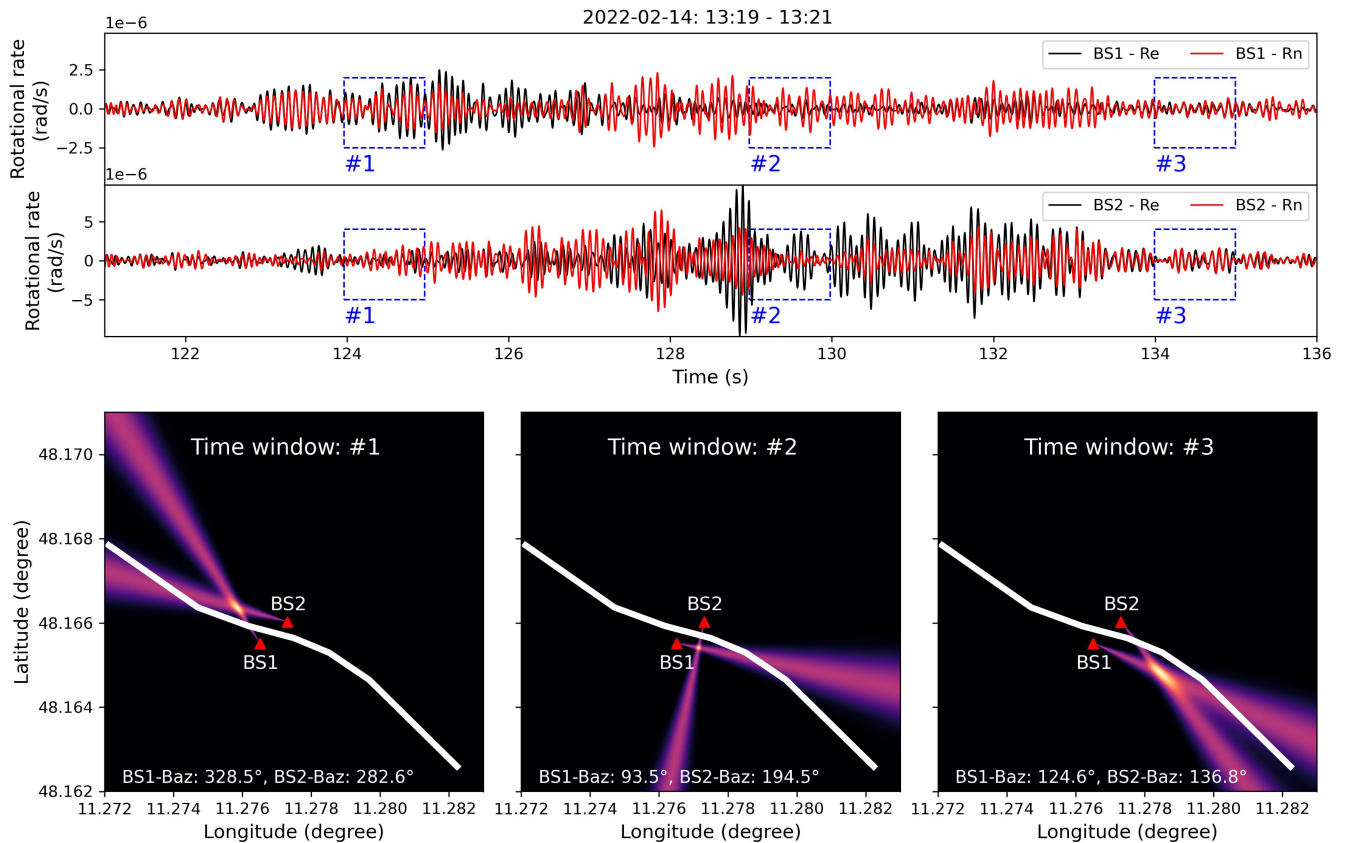
Figure 9 Top and middle: The horizontal rotational rates recorded at stations BS1 and BS2. Blue rectangles indicate the selected time windows for tracking moving vehicles. Bottom: The beamer plots correspond to the selected times shown in the top and middle panels. Brighter colors of the beams represent intersecting directions based on the estimated back azimuth at BS1 and BS2, calculated using Rayleigh waves and polarization method described in Section 4.2. The white curves denote the highway.

and Love waves (Yuan et al., 2020b), we can potentially implement a frequency-dependent attenuation model. This model may better capture the complexities of the near-surface, especially at higher frequencies where traffic noise becomes a significant factor.

Although the two types of rotational seismometers are among the most sensitive options available, they come at a higher cost compared to standard broadband seismometers (Bernauer et al., 2018; Yuan et al., 2020b). The ring laser gyroscope, in particular, is too bulky and expensive for seismological field observations (Igel et al., 2021). Typically, the cost of rotational sensors is proportional to their sensitivity and frequency range. However, in many urban and environmental applications, target signals are band-limited and possess higher energy levels than those observed in traditional earthquake studies. This presents an opportunity to develop specific, cost-effective portable rotational instruments using fiber-optic or alternative measurement principles (Smith, 2010; Brokešová and Málek, 2013; Cao et al., 2021).

9 Conclusions

We demonstrate that analyzing both translational and rotational ground motions together can effectively track moving seismic sources. The array-like capabilities of 6C measurements make this approach particularly

valuable in environments where deploying seismic arrays is difficult, such as on the ocean floor, in mountainous regions, or on planetary bodies. As a single-station method, 6C analysis provides a flexible alternative to traditional array measurements, allowing for the separation of different wavefield types, estimation of source directionality, and characterization of near-surface structures (Edme and Yuan, 2016; Wassermann et al., 2016). This method opens up new possibilities in seismology, especially in challenging environments and for continuous monitoring applications. The versatility of 6C measurements indicates their significant potential to enhance our understanding of various Earth processes and to improve monitoring systems for both natural and human-made events.

Acknowledgements

Data and code availability

Competing interests

The authors declare no competing interests and have fully disclosed all financial support for this project.

References

Almendros, J., Ibáñez, J. M., Alguacil, G., and Del Pezzo, E. Array analysis using circular-wave-front geometry: An application to locate the nearby seismo-volcanic source. *Geophysical Journal International*, 136(1):159–170, 1999. doi: 10.1046/j.1365-246X.1999.00699.x.

Asgari, S., Stafsudd, J. Z., Hudson, R. E., Yao, K., and Taciroglu, E. Moving source localization using seismic signal processing. *Journal of Sound and Vibration*, 335:384–396, 2015. doi: 10.1016/j.jsv.2014.09.027.

Bernauer, F., Wassermann, J., Guattari, F., Frenois, A., Bigueur, A., Gaillot, A., de Toldi, E., Ponceau, D., Schreiber, U., and Igel, H. BlueSeis3A: Full characterization of a 3C broadband rotational seismometer. *Seismological Research Letters*, 89(2A):620–629, 2018. doi: 10.1785/0220170143.

Brenguier, F., Clarke, D., Aoki, Y., Shapiro, N. M., Campillo, M., and Ferrazzini, V. Monitoring volcanoes using seismic noise correlations. *Comptes Rendus Geoscience*, 343(8-9):633–638, 2011. doi: 10.1016/j.crte.2010.12.010.

Brokešová, J. and Málek, J. Rotaphone, a self-calibrated six-degree-of-freedom seismic sensor and its strong-motion records. *Seismological Research Letters*, 84(5):737–744, 2013. doi: 10.1785/0220120189.

Burtin, A., Vergne, J., Rivera, L., and Dubernet, P. Location of river-induced seismic signal from noise correlation functions. *Geophysical Journal International*, 182(3):1161–1173, 2010. doi: 10.1111/j.1365-246X.2010.04701.x.

Cao, Y., Chen, Y., Zhou, T., Yang, C., Zhu, L., Zhang, D., Cao, Y., Zeng, W., He, D., and Li, Z. The development of a new IFOG-based 3C rotational seismometer. *Sensors*, 21(11):3899, 2021.

Chen, C., Wang, Y., Sun, L., Lin, C.-J., Wei, Y., Liao, C., Lin, B., and Qin, L. Six-Component Earthquake Synchronous Observations Across Taiwan Strait: Phase Velocity and Source Location. *Earth and Space Science*, 10(12):e2023EA003040, 2023. doi: 10.1029/2023EA003040.

Davy, C., Barruol, G., Fontaine, F. R., Sigloch, K., and Stutzmann, E. Tracking major storms from microseismic and hydroacoustic observations on the seafloor. *Geophysical Research Letters*, 41 (24):8825–8831, 2014. doi: 10.1002/2014GL062319.

Díaz, J., Ruiz, M., Sánchez-Pastor, P. S., and Romero, P. Urban seismology: On the origin of earth vibrations within a city. *Scientific reports*, 7(1):1–11, 2017. doi: 10.1038/s41598-017-15499-y.

Diaz, J., Ruiz, M., Udina, M., Polls, F., Martí, D., and Bech, J. Monitoring storm evolution using a high-density seismic network. *Scientific reports*, 13(1):1853, 2023. doi: 10.1038/s41598-023-28902-8.

Edme, P. and Yuan, S. Local dispersion curve estimation from seismic ambient noise using spatial gradients. *Interpretation*, 4(3): SJ17–SJ27, 2016. doi: 10.1190/INT-2016-0003.1.

Fan, W., McGuire, J. J., de Groot-Hedlin, C. D., Hedlin, M. A., Coats, S., and Fiedler, J. W. Stormquakes. *Geophysical Research Letters*, 46(22):12909–12918, 2019. doi: 10.1029/2019GL084217.

Fischer, J., Redlich, J.-P., Scheuermann, B., Schiller, J., Günes, M., Nagel, K., Wagner, P., Scheidgen, M., Zubow, A., Eveslage, I., et al. From earthquake detection to traffic surveillance–about information and communication infrastructures for smart cities. In *System Analysis and Modeling: Theory and Practice: 7th International Workshop, SAM 2012, Innsbruck, Austria, October 1-2, 2012. Revised Selected Papers 7*, pages 121–141. Springer, 2013.

Fuchs, F. and Bokelmann, G. Equidistant spectral lines in train vibrations. *Seismological Research Letters*, 89(1):56–66, 2018. doi: 10.1785/0220170092.

Gal, M. and Reading, A. M. Beamforming and polarization analysis. *Seismic Ambient Noise*, page 30, 2019. doi: 10.1017/9781108264808.004.

Gebauer, A., Tercjak, M., Schreiber, K. U., Igel, H., Kodet, J., Hugentobler, U., Wassermann, J., Bernauer, F., Lin, C.-J., Donner, S., et al. Reconstruction of the Instantaneous Earth Rotation Vector with Sub-Arcsecond Resolution Using a Large Scale Ring Laser Array. *Physical Review Letters*, 125(3):033605, 2020. doi: 10.1103/PhysRevLett.125.033605.

Greenhalgh, S., Sollberger, D., Schmelzbach, C., and Rutty, M. Single-station polarization analysis applied to seismic wavefields: A tutorial. *Advances in Geophysics*, 59:123–170, 2018. doi: 10.1016/bs.agph.2018.09.002.

Hadziioannou, C., Larose, E., Baig, A., Roux, P., and Campillo, M. Improving temporal resolution in ambient noise monitoring of seismic wave speed. *Journal of Geophysical Research: Solid Earth*, 116(B7), 2011. doi: 10.1029/2011JB008200.

Hadziioannou, C., Gaebler, P., Schreiber, U., Wassermann, J., and Igel, H. Examining ambient noise using colocated measurements of rotational and translational motion. *Journal of seismology*, 16(4):787–796, 2012. doi: 10.1007/s10950-012-9288-5.

Harris, C. R., Millman, K. J., Van Der Walt, S. J., Gommers, R., Virtanen, P., Cournapeau, D., Wieser, E., Taylor, J., Berg, S., Smith, N. J., et al. Array programming with NumPy. *Nature*, 585(7825): 357–362, 2020. doi: 10.1038/s41586-020-2649-2.

Heck, M., Hobiger, M., Van Herwijnen, A., Schweizer, J., and Fäh, D. Localization of seismic events produced by avalanches using multiple signal classification. *Geophysical Journal International*, 216(1):201–217, 2019. doi: 10.1093/gji/ggy394.

Hunter, J. D. Matplotlib: A 2D graphics environment. *Computing in science & engineering*, 9(03):90–95, 2007. doi: 10.1109/MCSE.2007.55.

Igel, H., Cochard, A., Wassermann, J., Flaws, A., Schreiber, U., Velikoseltsev, A., and Pham Dinh, N. Broad-band observations of earthquake-induced rotational ground motions. *Geophysical Journal International*, 168(1):182–196, 2007. doi: 10.1111/j.1365-246X.2006.03146.x.

Igel, H., Schreiber, K. U., Gebauer, A., Bernauer, F., Egdorf, S., Simonelli, A., Liny, C.-J., Wassermann, J., Donner, S., Hadziioannou, C., Yuan, S., Brotzer, A., Kodet, J., Tanimoto, T., Hugentobler, U., and Wells7, J.-P. R. ROMY: A Multi-Component Ring Laser for Geodesy and Geophysics. *Geophysical Journal International*, 01 2021. doi: 10.1093/gji/ggaa614. ggaa614.

Kedar, S. and Webb, F. H. The ocean's seismic hum. *Science*, 307 (5710):682–683, 2005. doi: 10.1126/science.1108380.

Keil, S., Wassermann, J., and Igel, H. Single-station seismic microzonation using 6C measurements. *Journal of Seismology*, 25: 103–114, 2021. doi: 10.1007/s10950-020-09944-1.

Krim, H. and Viberg, M. Two decades of array signal processing re-

search: the parametric approach. *IEEE signal processing magazine*, 13(4):67–94, 1996. doi: 10.1109/79.526899.

Langston, C. A. Spatial gradient analysis for linear seismic arrays. *Bulletin of the Seismological Society of America*, 97(1B):265–280, 2007. doi: 10.1785/0120060100.

Lindsey, N. J. and Martin, E. R. Fiber-optic seismology. *Annual Review of Earth and Planetary Sciences*, 49(1):309–336, 2021. doi: 10.1146/annurev-earth-072420-065213.

Liu, H., Ma, J., Xu, T., Yan, W., Ma, L., and Zhang, X. Vehicle Detection and Classification Using Distributed Fiber Optic Acoustic Sensing. *IEEE Transactions on Vehicular Technology*, 69(2): 1363–1374, 2019. doi: 10.1109/TVT.2019.2962334.

Manconi, A., Picozzi, M., Coviello, V., De Santis, F., and Elia, L. Real-time detection, location, and characterization of rockslides using broadband regional seismic networks. *Geophysical Research Letters*, 43(13):6960–6967, 2016. doi: 10.1002/2016GL069572.

Margheriti, L., Nostro, C., Cocina, O., Castellano, M., Moretti, M., Lauciani, V., Quintiliani, M., Bono, A., Mele, F. M., Pintore, S., et al. Seismic surveillance and earthquake monitoring in Italy. *Seismological Research Letters*, 92(3):1659–1671, 2021.

Martin, E., Lindsey, N., Dou, S., Ajo-Franklin, J., Daley, T., Freifeld, B., Robertson, M., Ulrich, C., Wagner, A., and Bjella, K. Interferometry of a roadside DAS array in Fairbanks, AK. In *SEG Technical Program Expanded Abstracts 2016*, pages 2725–2729. Society of Exploration Geophysicists, 2016. doi: 10.1190/segam2016-13963708.1.

Megies, T., Beyreuther, M., Barsch, R., Krischer, L., and Wassermann, J. ObsPy–What can it do for data centers and observatories? *Annals of Geophysics*, 54(1):47–58, 2011. doi: 10.3929/ethz-b-000130217.

Nakata, N. Near-surface S-wave velocities estimated from traffic-induced Love waves using seismic interferometry with double beamforming. *Interpretation*, 4(4):SQ23–SQ31, 2016. doi: 10.1190/INT-2016-0013.1.

Obermann, A., Planes, T., Larose, E., and Campillo, M. Imaging preeruptive and coeruptive structural and mechanical changes of a volcano with ambient seismic noise. *Journal of Geophysical Research: Solid Earth*, 118(12):6285–6294, 2013. doi: 10.1002/2013JB010399.

Obermann, A., Froment, B., Campillo, M., Larose, E., Planes, T., Valette, B., Chen, J., and Liu, Q. Seismic noise correlations to image structural and mechanical changes associated with the Mw 7.9 2008 Wenchuan earthquake. *Journal of Geophysical Research: Solid Earth*, 119(4):3155–3168, 2014. doi: 10.1002/2013JB010932.

Reinwald, M., Moseley, B., Szenicer, A., Nissen-Meyer, T., Oduor, S., Vollrath, F., Markham, A., and Mortimer, B. Seismic localization of elephant rumbles as a monitoring approach. *Journal of the Royal Society Interface*, 18(180):20210264, 2021. doi: 10.1098/rsif.2021.0264.

Riahi, N. and Gerstoft, P. The seismic traffic footprint: Tracking trains, aircraft, and cars seismically. *Geophysical Research Letters*, 42(8):2674–2681, 2015. doi: 10.1002/2015GL063558.

Smith, D. ATA's nanoradian-class rotational sensors. In *Second IWGoRS Workshop, October*, pages 11–13, 2010.

Spudich, P., Steck, L. K., Hellweg, M., Fletcher, J., and Baker, L. M. Transient stresses at Parkfield, California, produced by the M 7.4 Landers earthquake of June 28, 1992: Observations from the UPSAR dense seismograph array. *Journal of Geophysical Research: Solid Earth*, 100(B1):675–690, 1995. doi: 10.1029/94JB02477.

Suriñach Cornet, E., Vilajosana Guillén, I., Khazaradze, G., Bi-

escas Górriz, B., Furdada i Bellavista, G., and Vilaplana, J. M. Seismic detection and characterization of landslides and other mass movements. *Natural Hazards and Earth System Sciences, 2005, Vol. 5, p. 791-798*, 2005. doi: 10.5194/nhess-5-791-2005.

Tape, C., Ringler, A. T., and Hampton, D. L. Recording the aurora at seismometers across Alaska. *Seismological Research Letters*, 91 (6):3039–3053, 2020. doi: 10.1785/0220200161.

Tonnellier, A., Helmstetter, A., Malet, J.-P., Schmittbuhl, J., Corsini, A., and Joswig, M. Seismic monitoring of soft-rock landslides: the Super-Sauze and Valoria case studies. *Geophysical Journal International*, 193(3):1515–1536, 2013. doi: 10.1093/gji/ggt039.

Valero, M., Li, F., and Song, W. Smart seismic network for shallow subsurface imaging and infrastructure security. *International Journal of Sensor Networks*, 31(1):10–23, 2019.

Venkatraman, D., Reddy, V., and Khong, A. W. A study of the ambiguity problem in footstep bearing estimation using tri-axial geophone. In *2011 8th International Conference on Information, Communications & Signal Processing*, pages 1–5. IEEE, 2011. doi: 10.1109/ICICS.2011.6173512.

Wang, H., Quan, W., Wang, Y., and Miller, G. R. Dual roadside seismic sensor for moving road vehicle detection and characterization. *Sensors*, 14(2):2892–2910, 2014. doi: 10.3390/s140202892.

Wassermann, J., Wietek, A., Hadziioannou, C., and Igel, H. Toward a single-station approach for microzonation: Using vertical rotation rate to estimate Love-wave dispersion curves and direction finding. *Bulletin of the Seismological Society of America*, 106 (3):1316–1330, 2016. doi: 10.1785/0120150250.

Yuan, S. Shihao-Yuan/6C-source-tracking: Tracking vehicle sources using six-component single-station seismic measurements (v1.0.0). *Zenodo*, 2024. doi: 10.5281/zenodo.14017149.

Yuan, S., Gessele, K., Gabriel, A.-A., May, D. A., Wassermann, J., and Igel, H. Seismic source tracking with six degree-of-freedom ground motion observations. *Journal of Geophysical Research: Solid Earth*, page e2020JB021112, 2020a. doi: 10.1029/2020JB021112.

Yuan, S., Simonelli, A., Lin, C.-J., Bernauer, F., Donner, S., Braun, T., Wassermann, J., and Igel, H. Six Degree-of-Freedom Broadband Ground-Motion Observations with Portable Sensors: Validation, Local Earthquakes, and Signal Processing. *Bulletin of the Seismological Society of America*, 110(3):953–969, 2020b. doi: 10.1785/0120190277.

Zhao, Y., Nilot, E. A., Li, B., Fang, G., Luo, W., and Li, Y. E. Seismic attenuation extraction from traffic signals recorded by a single seismic station. *Geophysical Research Letters*, 50(3): e2022GL100548, 2023. doi: 10.1029/2022GL100548.